RESEARCH   **Open Access**

Flexural Capacity and Behaviour of Geopolymer Concrete Beams Reinforced with Glass Fibre-Reinforced Polymer Bars

Hemn Qader Ahmed[*] , Dilshad Kakasor Jaf and Sinan Abdulkhaleq Yaseen

Abstract

Geopolymer concrete (GPC) with Glass fibre-reinforced polymer (GFRP) bars can provide a better construction system with high sustainability, high durability, and adequate strength. Few studies deal with the combination of these materials. The present investigation obtains the flexural capacity and behaviour of GPC and ordinary Portland concrete beams reinforced with GFRP bars (GFRP-RGPC and GFRP-ROPC, respectively). Twelve beams consisting of nine GFRP-RGPC and three GFRP-ROPC beams were cast and tested by using the four-point bending test over an active span of 2000 mm. Rebar ratio, compressive strength, and concrete types were taken as the variables. Initial cracking load, ultimate load capacity, load–deflection behaviour, Load–strain curves, crack width, the number of cracks and failure modes, were studied. Experimental results of beams were compared with the proposed equations provided by ACI 440.1R-15, CSA S806-12, and parabolic stress block method. The Results showed the decrease of deflection and increase of first cracking load by increasing the compressive strength. A slight increase in the deflection of GFRP-RGPC beams and approximately the same value of ultimate load were observed. GFRP-RGPC beams also recorded a higher value of crack width compared with GFRP-ROPC beams. The parabolic stress block method predicted the flexural capacity of the beams close to the experimental results rather than ACI 440.1R-15 and CSA S806-12.

Keywords: flexural capacity, geopolymer concrete, glass fibre-reinforced polymer bar

1 Introduction

Regular ordinary Portland cement has been used as a binder for producing ordinary Portland concrete (OPC) for a long time. The demand for OPC is expected to increase in the future due to the rise of infrastructure requirement of many developing countries and the increasingly old and deteriorated concrete structures requiring urgent repair and rehabilitation. However, the production of Portland cement contributes billions of tons of waste materials and approximately 7% of the world's greenhouse gases every year (Mehta 2001). Several environmental problems have been indicated at some stages in the production of Portland cement due to

the calcination of limestone and burning of fossil gases. The quantity of the carbon dioxide (CO_2) that launches in the atmosphere throughout the manufacture of Portland cement is in the order of 1 ton during the production of 1 ton of Portland cement (Hardjito and Rangan 2005; McCaffrey 2002; Madhava et al. 2013). Davidovits (1988) discovered an alkaline activator liquid. The activator could be used to react with silicon and the aluminium in materials of geological origin source or fly ash and rice husk ash (by-product materials) and produce binders. The term 'geopolymer' is coined to represent those binders. Geopolymer concrete (GPC) is a type of concrete that no longer uses any cement in its manufacturing (Hardjito and Wallah 2005, Kar et al. 2014). GPC has attracted considerable attention from researchers because of its remarkable potential compared with OPC. Researchers are moving their focus on from chemistry

*Correspondence: hemn.ahmed@su.edu.krd
Civil Engineering Department, Salahaddin University -Erbil, Erbil, Iraq

Ahmed *et al. Int J Concr Struct Mater* (2020) 14:14

Page 2 of 16

to engineering and the commercial production of GPC (Lloyd and Rangan 2010; Kotwal et al. 2015). Geopolymer binder produced by a synthesis of Silica and Alumina rich pozzolanic precursor-like Fly Ash, with the alkaline solution as an activator through the process of Geopolymerization, and have become known as a promising option to conventional cement (Luhar et al. 2019).

The mechanical strength of the GPC system depends on several factors. The pH of the activating solution is the primary parameter that controls the compressive strength of a GPC. According to (Khale and Chaudhary 2007), the activating solution with a pH range of 13–14 is the most suitable for the formation of the GPC with better mechanical strength. The properties of source materials also affect the strength of GPC. High reactivity source materials lead to produce geopolymer systems with higher strength (Xu and Van Deventer 2002). The early strength development of geopolymer system can be enhanced by using higher molarity of NaOH, but with low alkali content and by using elevated temperature for curing (Khale and Chaudhary 2007). Duxson et al. (2007) reported that other desirable characteristics of GPC such as; rapid development of mechanical strength, fire resistance, dimensional stability, acid resistance, excellent adherence to aggregates and reinforcements, and have lower material cost, approximately 10–30% lower than that of OPC (Duxson et al. 2007). The chemical structure determines the type of application of geo-polymeric materials in terms of Silica-to-Alumina (Si:Al) Atomic ratio in the polysialate. Davidovits (1994) classified the application types according to the Si:Al ratio as follows: For Si:Al ratio (1): Applications (Bricks, Ceramics and Fire protection). For Si:Al ratio (2): Applications (Low CO_2 cements and concretes and Radioactive and toxic waste encapsulation). For Si:Al ratio (3): Applications (Fire protection fibre glass composite, Foundry equipments, Heat resistant composites, 200 °C to 1000 °C and Tooling for aeronautics titanium process). For Si:Al ratio (>3): Applications(Sealants for industry, 200 °C to 600 °C and Tooling for aeronautics SPF aluminium). For Si:Al ratio (20–35): Applications(Fire resistant and heat resistant fibre composites). For many applications in the civil engineering field a low Si:Al ratio is suitable (Davidovits 1994).

Moreover, the alkalinity of concrete protects the steel reinforcement (non-prestressed and prestressed) from corrosion, thereby usually resulting in durable and serviceable construction. Structures are subjected to violent environments, including marine systems and bridges and parking garages, which have been exposed to deicing salts. The combination of moisture, temperature, and chlorides reduce the concrete alkalinity and cause the corrosion of reinforcing steel. Finally, the corrosion

action causes concrete deterioration and inability of concrete serviceability. To solve this corrosion problem; professionals have used composite substances made of fibres embedded in a polymeric resin called fibre-reinforced polymer (FRP) bars (ACI 440.1R-15 2015). FRP substances are non-magnetic and non-corrosive; thus, the issues of electromagnetic interference and metal corrosion can be prevented with FRP reinforcement. Besides, FRP materials show considerable residences, such as excessive tensile stress, which make them suitable for use as structural reinforcement (Theriault and Benmokrane 1998). Fibre-reinforced polymer bars do not exhibit any yielding before failure. Thus when FRP bars experience tensile forces more extensive than the tensile strength, fail by rupture and splitting of the fibres occur. The tensile behaviour of FRP reinforcement is dependent on a number of factors especially the fibre volume to the total volume of the FRP reinforcement (fibre-volume fraction). By altering this fraction, the strength and stiffness of FRP bars can be changed (Fico 2007). Other noticeable influences include the properties and types of matrices used to bond and protect the fibres and the level of quality control during manufacturing (Wu 1990).

GPC reinforced with GFRP bars has a bond strength similar to that of steel-reinforced GPC, and they can be an effective alternative as internal reinforcement for geopolymer concrete structures (Maranan et al. 2014). The mechanical interlock and friction force resistance provided by the sand coating, bonded on the surface of the GFRP bars, were found to be adequate to secure a composite action between the bars and the geopolymer concrete (Maranan et al. 2015). Due to the lower elastic modulus of GFRP bars, beams reinforced with these bars exhibit low post cracking flexural stiffness compared to the concrete beams conventionally reinforced with steel bars (Ascione et al. 2010).

Several investigations have been conducted on the flexural capacity of steel-reinforced GPC (SRGPC) beams (Kumaravel and Thirugnanasambandam 2013; Madheswaran et al. 2014; Hutagi and Khadiranaikar 2016; Kumar and Ramesh 2017). The load–deflection relationship obtained from steel-reinforced OPC (SROPC) and SRGPC beams are almost similar with a slightly higher ultimate load in SRGPC beams. The first cracking load of SRGPC beams is better than that of SROPC beams, which shows better load carrying strength (Thangamanibindhu and Murthy 2015). The failure of SRGPC beams is more ductile than that of SROPC beams, wherein SRGPC beams exhibit a higher number of small cracks compared with SROPC beams (Abraham et al. 2013). Maranan et al. (2015) investigated the flexural capacity of glass fibre-reinforced polymer-RGPC beams; the authors concluded that the bar diameter had no

Ahmed *et al. Int J Concr Struct Mater* (2020) 14:14

Page 3 of 16

notable effect on the flexural capacity of the beams. The serviceability behaviour of a beam was enhanced with the increasing rebar ratio (Maranan et al. 2015). Shear behaviour of geopolymer concrete beams reinforced with glass fibre-reinforced polymer (GFRP) bars and stirrups studied by (Maranan et al. 2017). The authors concluded that the GFRP stirrups enhanced both the shear strength and deflection capacity of the beams by approximately 200%.

Geopolymer concrete and glass fibre-reinforced polymer (GFRP) bars can provide a good construction system by utilising the advantages of both materials. Few studies have combined these materials, and this is the principal topic of the present study, in which the flexural capacity and behaviour of fly ash-based GFRP-RGPC beams were investigated. The studied parameters were compressive strength, rebar ratio with respect to the balanced rebar ratio and concrete types (namely, RGPC and ROPC). The crack pattern, failure modes, load–deflection curves, and Load–strain curves were presented. Moreover, experimental results were compared with the predicted flexural strength by using the Equations proposed by (ACI 440.1R-15 2015) and (CSA S806–12 2012), and parabolic stress block method.

2 Materials and Methods
2.1 Design of Beam Specimens and Program
The beam specimens were designed according to (ACI 440.1R-15 2015). The experimental program consisted of nine GFRP-RGPC and three GFRP-ROPC beams with target compressive strengths of 20, 35 and 50 MPa. The beams were divided into four groups, with three beams in each group. Groups 1–4 consisted of GFRP-RGPC (20 MPa), GFRP-RGPC (35 MPa), GFRP-RGPC (50 MPa) and GFRP-ROPC (50 MPa), respectively. GFRP bars of 6 mm (A_f = 28 mm^2), with ultimate tensile strength f_{fu} = 1280 MPa, modulus of elasticity E_f = 46 GPa, and the ultimate strain of 2.7% was used as a reinforcement for all the beam specimens. All groups share the same height and width of 300 mm and 160 mm, respectively. The different rebar ratio conditions ρ_f with respect to the balanced rebar ratio ρ_{fb} were obtained in each group. rebar ratio conditions ($\rho_f < \rho_{fb}$, $\rho_{fb} < \rho f < 1.4 \, \rho_{fb}$ and $\rho_f > 1.4 \, \rho_{fb}$), due to the limitations of (ACI 440.1R-15 2015) in maintaining the three failure modes. Failure modes; tension failure of GFRP bars, tension failure of GFRP bars followed by the compression failure of the top concrete part and compressive failure of the top concrete part. A clear cover was maintained at 20 mm for all beams. The length of the beams was varied (2200–2500 mm) due to the requirement of development length. Regular deformed steel bars with a diameter of 6 mm were used as a longitudinal reinforcement at the top in shear spans and as vertical stirrups. Stirrups were placed in the centre-to-centre spacing of 100 mm to prevent shear failure in the beams. The beams were simply supported over an effective span of 2000 mm. Figure 1 and Table 1 show the details of the specimens and the test program, respectively.
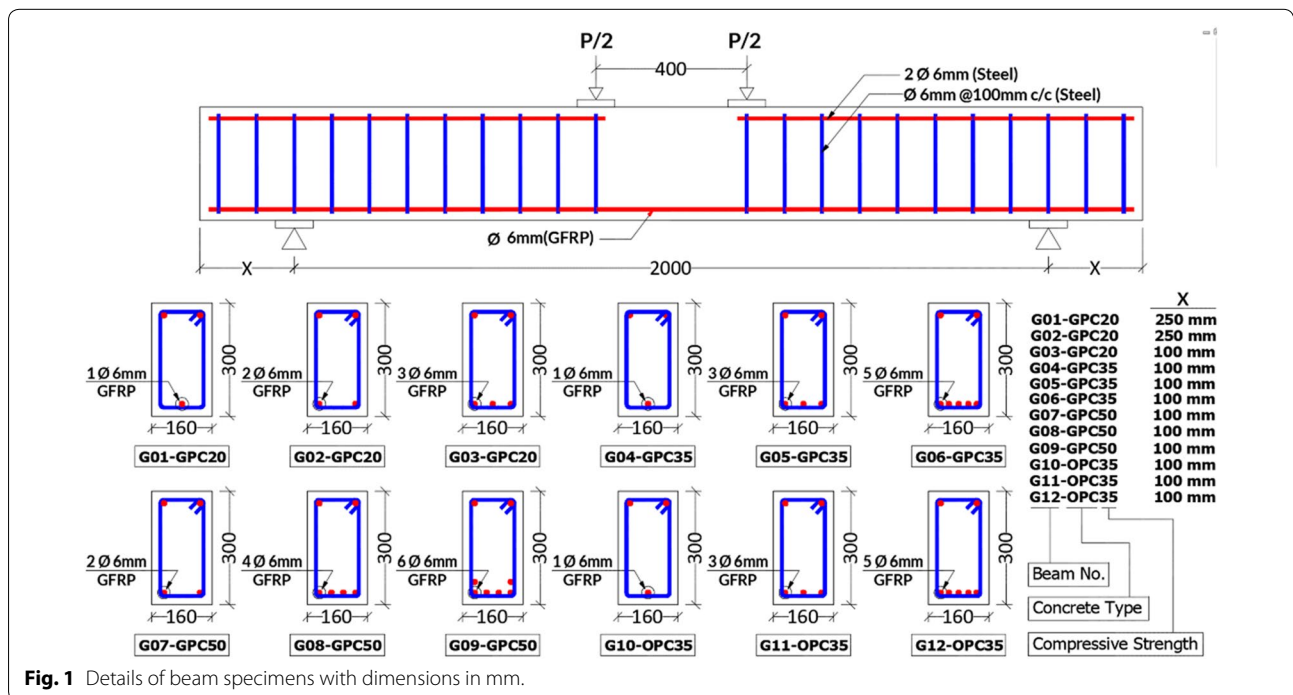

Fig. 1 Details of beam specimens with dimensions in mm.

Ahmed *et al. Int J Concr Struct Mater* (2020) 14:14

Page 4 of 16

Table 1 Test program.

Group	Beam ID	Concrete type	Compressive strength f'_c (MPa)	Rebar ratio condition ρ_f
G 1	G01-GPC20	GPC	20	0.63 ρ_{fb}
	G02-GPC20			1.22 ρ_{fb}
	G03-GPC20			1.52 ρ_{fb}
G 2	G04-GPC35		35	0.44 ρ_{fb}
	G05-GPC35			1.38 ρ_{fb}
	G06-GPC35			2.20 ρ_{fb}
G3	G07-GPC50		50	0.69 ρ_{fb}
	G08-GPC50			1.40 ρ_{fb}
	G09-GPC50			2.16 ρ_{fb}
G4	G10-OPC35	OPC	35	0.36 ρ_{fb}
	G11-OPC35			1.08 ρ_{fb}
	G12-OPC35			1.88 ρ_{fb}

2.2 Material, Mix Proportion, and Preparation of GPC

The alkaline liquid preparation materials used in this study were; sodium silicate solution (Na_2SiO_3), which is available in liquid gel form with a chemical composition of 13.4% Na_2O, 32.5% SiO_2 and 54.1% water, and sodium hydroxide (NaOH) pellets with 98% purity, which are presented in flakes and pellets. For the preparation of GPC, the materials were low-calcium fly ash type-F coarse aggregates with a maximum size of 9.52 mm and fine aggregates. The grading of aggregates satisfied the limits provided by (ASTM C33 2003). Sulfonated naphthalene formaldehyde as superplasticiser was used to enhance the workability.
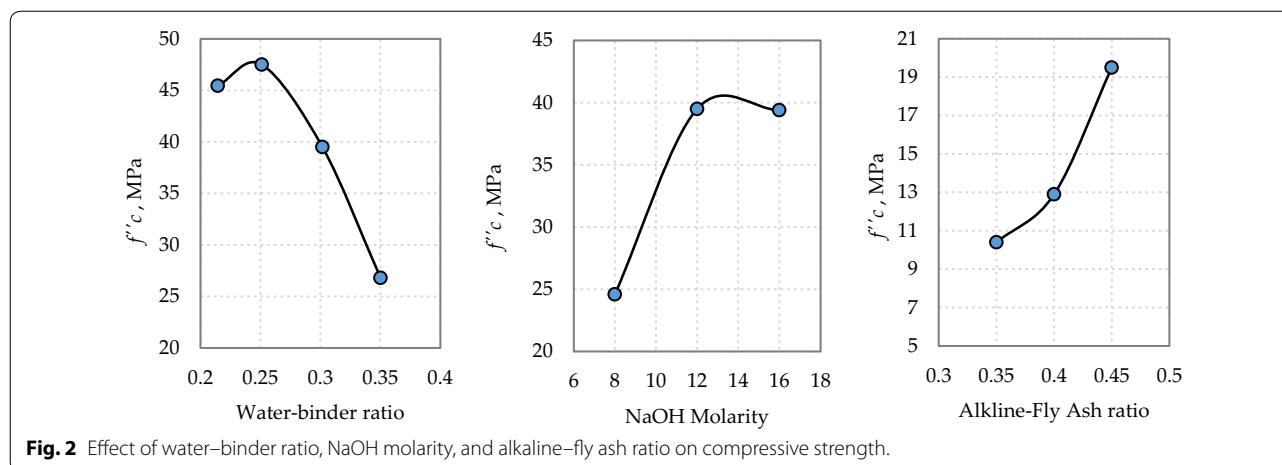
Geopolymer concrete has only been discovered recently. Hence, no fixed mix design exists for GPC. In this study, 13 trail mixes were conducted to achieve the required compressive strength of RGPC and ROPC beams. The variables considered for the GPC trail mixes were; molarity of sodium hydroxide (M), alkaline-fly ash ratio and water-binder ratio. The water–cement ratio was the only variable considered for OPC trails. Table 2 shows the details of the trail mix proportions. Each trail consists of nine 100 mm × 200 mm cylinders, which were tested according to (ASTM C 39/C 39M 1999) after 28 days. Increasing molarity of sodium hydroxide caused to increase compressive strength up to 12 M, but when increased to 16 M compressive strength decreased—when alkaline-fly ash ratio increased caused to increase in the compressive strength. The excess presence of NaOH (hydroxide ions) leads to fast and early precipitation of aluminosilicates gel, which hardens rapidly and also inhibits the formation of other geopolymeric precursors (Lee and van Deventer 2002). The optimum water-binder ratio was 0.25. Figure 2 shows the effect of trail mix parameters on compressive strength.

The difference between OPC and GPC is related to the binder portion. The OPC binder consists of cement and water, whereas fly ash-based GPC consists of fly ash, alkaline activator, and additional water. The alkaline liquid was prepared a day before casting. Firstly, the sodium hydroxide was dissolved in water, based on required molarity (M). For example, 480 g was the required amount of sodium hydroxide to be dissolved in water to obtain 1 L of sodium hydroxide solution. ($12 \times$ molecular weight of sodium hydroxide (4) = 480 g), and 1330 g was

Table 2 Trail mix proportion details and results.

Mix	G (kg/m³)	S (kg/m³)	FA (kg/m³)	M	S/S	A/F	C (kg/m³)	EW (kg/m³)	SP % (kg/m³)	W/B ratio	W/C ratio	Compressive strength, f'_c (MPa)
T01	1230	660	400	12	2.5	0.45		0	3	0.2145		45.5
T02	1230	660	400	12	2.5	0.45		32	2	0.3017		39.5
T03	1230	660	400	12	2.5	0.45		14	2	0.2511		47.5
T04	1230	660	400	12	2.5	0.45		48	2	0.3502		26.8
T05	1230	660	400	16	2.5	0.45		36	2	0.3009		39.4
T06	1230	660	400	8	2.5	0.45		27	2	0.3019		24.6
T07	1230	660	400	8	2.5	0.45		43	2	0.3504		19.5
T08	1230	660	400	8	2.5	0.4		50	2	0.3512		12.9
T09	1230	660	400	8	2.5	0.35		57	2	0.3521		10.4
T10	1230	660	400	12	2.5	0.45		38	2	0.3195		34.5
T11	1230	660					400				0.3	52.2
T12	1230	660					400				0.4	36.1
T13	1230	660					400				0.5	25.7

G coarse aggregate, *S* sand, *FA* fly ash, *M* molarity of sodium hydroxide, *S/S* sodium silicate–sodium hydroxide ratio, *A/F* alkaline-fly ash ratio, *C* cement, *EW* extra water, *SP* superplasticizer, *W/B* water-binder ratio, *W/C* water–cement ratio.

Ahmed *et al. Int J Concr Struct Mater*   (2020) 14:14

Page 5 of 16

Fig. 2 Effect of water–binder ratio, NaOH molarity, and alkaline–fly ash ratio on compressive strength.

the experimentally determined weight of 1 L of sodium hydroxide for M12. Secondly, sodium silicate and sodium hydroxide solutions were mixed in a ratio of 2.5:1, which is the best ratio on the basis of a previous study (Hardjito and Rangan 2005). The water–binder ratio was calculated as follows; the amount of water in sodium silicate solution, sodium hydroxide solution, and additional water was divided by the solid parts in sodium silicate solution, sodium hydroxide solution and fly ash.

At casting day, the aggregates were initially placed in an electric mixer. Subsequently, half of the additional water was added and mixed for 5 min, and fly ash was then added and mixed for an extra 5 min. After that, the alkaline liquid was added to the mixture. Finally, the remaining additional water and superplasticiser of 2% of the weight of fly ash were added. The fresh GPC cast into steel moulds which were coated internally with special tape to avoid the GPC from sticking to the mould. A rest period of 60 min was considered before placing the casted GPC into an oven and cured for 24 h at a temperature of 70 °C. In this study, the oven-dry method was used for curing the GPC.

2.3 Casting Beam Specimen and Test Method
From the trail mix results, T03, T07 and T10 were selected for casting GFRP-RGPC beams and T12 for GFRP-ROPC beams. Before casting, reinforcement was prepared, including the attachment of strain gauges. The gauge locations on the bars were initially smoothened and cleaned. The strain gauges were then bonded to the prepared surface of the FRP bars with an adhesive material. Subsequently, heat resistant wires were soldered to the strain gauges. Finally, the strain gauges were covered by a heat resistant protective tape. The casting moulds, including a steel mould, three 150 mm × 300 mm cylinders and three 75 mm × 75 mm × 400 mm prisms, were

used for casting the control specimens of GFRP-RGPC beams. The mould, cylinders, and prisms were internally coated with a special tape for the same reason mentioned earlier and then placed on an external vibrator. After casting, the specimens were left for 60 min as a rest period and then placed into the oven and cured for 24 h at 70 °C. The following day, the specimens were demoulded and placed in a laboratory environment until the test day. The classic method was used for casting and curing of the GFRP-ROPC beams. Figure 3 shows the GFRP-RGPC and GFRP-ROPC beams.

A four-point static bending test method was used in this study, as shown in Fig. 4. The beams were loaded at mid-span with two concentrated loads spaced at 400 mm. The load was applied by a hydraulic jack with strength and approximate rate of 2500 kN and 2 kN/min, respectively. The mid-span deflection was measured using a dial gauge and camera recorder. Furthermore, a data logger was used for recording strains in the electrical strain gauges that were attached on the top surface of the beams and the GFRP bars. A crack measurement sensor was also used for recording the crack width.

3 Results and Discussion
3.1 Summary of Test Results and Control Specimens
Table 3 presents the test results for the Initial cracking load, ultimate load, deflection, and failure modes. For the same compressive strength and rebar condition, the ultimate load values of GFRP-RGPC and GFRP-ROPC beams were almost similar, except for beams with $\rho_f > 1.4$ ρ_{fb} which GRFP-ROPC recorded slightly higher value. The rebar ratio had a remarkable effect on first cracking load and ultimate load of each group. The results showed that the enhancement of deflection and the initial cracking load was obtained by increasing the compressive strength, wherein deflection of GFRP-RGPC was

Ahmed *et al. Int J Concr Struct Mater* (2020) 14:14

Page 6 of 16

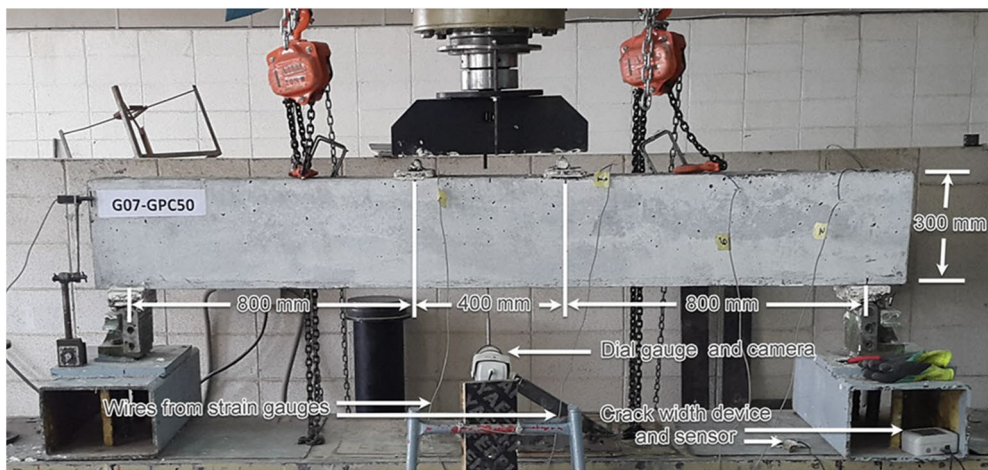**Fig. 3** **a** GFRP-RGPC beams, **b** GFRP-ROPC beams.

Fig. 4 Test setup.

Table 3 Results of the tested Beams.

Group	Beam ID	First crack load P_{cr} (kN)	Ultimate load P_u (kN)	Deflection Δ (mm)	Failure mode
G 1	G01-GPC20	4.30	26.3	29.34	Tension failure of GFRP bars
	G02-GPC20	4.70	56.5	42.12	Tension failure of GFRP bars
	G03-GPC20	11.70	81.7	39.83	Tension failure of GFRP bars followed by compressive failure of the top concrete part
G 2	G04-GPC35	11.9	35.8	25.13	Tension failure of GFRP bars
	G05-GPC35	12.40	88.3	39.35	Tension failure of GFRP bars followed by compressive failure of the top concrete part
	G06-GPC35	15.50	124.7	36.80	Tension failure of GFRP bars followed by compressive failure of the top concrete part
G3	G07-GPC50	18.30	57.7	28.42	Tension failure of GFRP bars
	G08-GPC50	20.8	100.0	28.98	Tension failure of GFRP bars followed by compressive failure of the top concrete part
	G09-GPC50	22.60	145.8	35.17	Compressive failure of the top concrete part
G4	G10-OPC35	15.50	34.2	17.66	Tension failure of GFRP bars
	G11-OPC35	20.00	84.4	31.00	Tension failure of GFRP bars followed by compressive failure of the top concrete part
	G12-OPC35	20.90	137.8	41.14	Debonding of GFRP from the concrete at the bottom of the beam

slightly higher. Furthermore, four different failure modes were observed. Failure modes namely; tension failure of GFRP bars, tension failure of GFRP bars followed by the compression failure of the top concrete part, compressive failure of the top concrete part and debonding of GFRP from the concrete at the bottom of the beam. The control specimens of each beam were tested at the same age of the tested beam. Three cylinders were tested according to (ASTM C 39/C 39M 1999) for concrete compressive strengths. Three cylinders were tested according to (ASTM C 496/C 496M 2004) for splitting tensile strengths and three prisms were tested for flexural strength of concrete (ASTM C 78/C 78M 2013). Furthermore, the elastic modulus of GPC was obtained by testing the three cylinders according to (ASTM C 469/C 469M 2014), and the density of each mix was calculated based on cylinders and prisms. Table 4 shows the results of the control specimens.

3.2 Crack Pattern and Failure Mode

Figures 5 and 6 show the typical failure modes of beams and the failure crack patterns for all the beams, respectively. The difference in crack patterns and failure modes was due to the rebar ratio, compressive strength of the concrete and types of concrete (namely, GPC and OPC). The prediction failure modes provided by (ACI 440.1R-15 2015) satisfied with the experimental failure modes of the beams in this study by 66.667%. The difference referred to the criticality of transition failure mode, GPC type of concrete and the ultimate strain assumption of concrete by (ACI 440.1R-15 2015). Before loading, all the beam specimens were initially free of cracks. The Initial cracking of the GFRP-RGPC and GFRP-ROPC beams was observed in the constant moment region exactly under the applied point load. The Initial cracking load in the GFRP-ROPC beams was slightly higher than that in the GFRP-RGPC beams due to a small difference in concrete compressive strength and concrete types. After the first cracking, new cracks were formed, and the crack width continued to enlarge with the applied load in GFRP-RGPC and GFRP-ROPC beams. At maximum load, both GFRP-RGPC and GFRP-ROPC beams recorded approximately the same amount of cracks (number of cracks). The crack width in the GFRP-RGPC beams was also more extensive than that in the GFRP-ROPC beams, except beams with $\rho_f < \rho_{fb}$.

Table 4 Results of control specimens.

Group	Beam ID	Compressive strength f'_c (Mpa)	Splitting tensile strength f_{ct} (Mpa)	Modulus of Rupture f_r (Mpa)	Modulus of elasticity E_c (Mpa)	Density kg/m³
G 1	G01-GPC20	19.89	1.693	3.44	18,267	2406
	G02-GPC20	20.67	1.568	3.27	17,821	2372
	G03-GPC20	26.05	1.848	2.81	15,393	2400
G 2	G04-GPC35	31.37	2.287	3.57	29,205	2409
	G05-GPC35	29.62	2.497	4.40	24,337	2373
	G06-GPC35	33.45	2.131	3.51	27,596	2330
G3	G07-GPC50	46.28	3.599	4.81	29,066	2427
	G08-GPC50	45.12	3.167	4.92	26,691	2387
	G09-GPC50	45.44	3.272	4.46	25,771	2370
G4	G10-OPC35	34.62	2.892	3.57	28,534	2453
	G11-OPC35	34.62	2.892	3.57	28,534	2453
	G12-OPC35	34.62	2.892	3.57	28,534	2453

Fig. 5 Typical failure modes: **a** tension failure of GFRP bars, **b** tension failure of GFRP bars followed by compressive failure of the top concrete part, **c** compressive failure of the top concrete part and **d** debonding of GFRP from the concrete at the bottom of the beam.

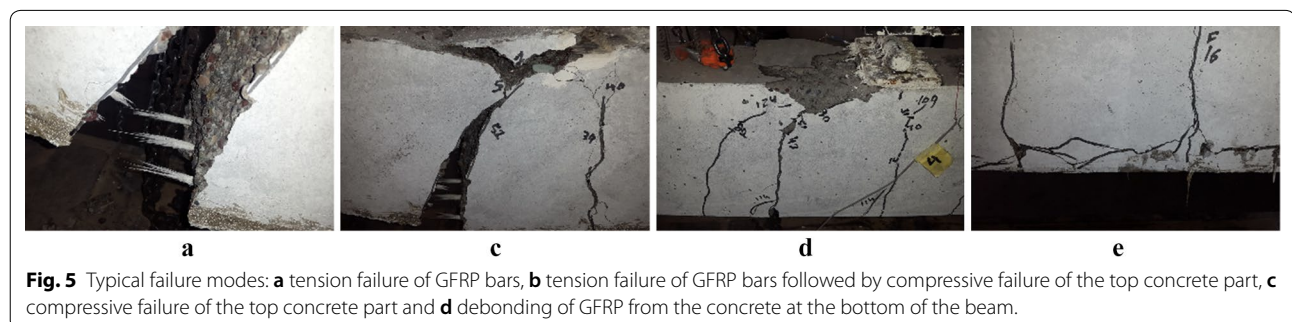Ahmed *et al. Int J Concr Struct Mater*   (2020) 14:14

Page 8 of 16

Fig. 6 Crack pattern and failure mode.

Figure 6a, b, d, g, j respectively show that beams G01-GPC20, G01-GPC20, G04-GPC35, G07-GPC50 and G10-OPC35 failed due to the rupture of the FRP bars (tension failure of GFRP bars). This type of failure occurred for beams with a rebar ratio condition of $\rho_f < \rho_{fb}$. The failure location in beams G01-GPC20, G02-GPC20 and G07-GPC50, was precisely in the midspan' whereas that in beams G10-OPC35 and G10-OPC35 was under the point load location, and a few cracks and a higher value of crack width were also recorded. These cracks were mainly classified as vertical flexural cracks, which were perpendicular to the longitudinal axis of the beam.

Figure 6c, e, f, h, k respectively illustrate that beams G03-GPC20, G05-GPC35, G06-GPC35, G08-GPC50, and G11-OPC35 failed due to the crushing of concrete under the load, which propagated instantaneously. Failure type: tension failure of GFRP bars followed by the compressive failure of the top concrete part). Similarly, cracking was initiated when the applied moment reached the cracking moment. Cracking consisted of vertical cracks perpendicular to the direction of the principal tensile stress induced by pure moment. As the load increased, flexural cracks reached into the shear span.

Ahmed *et al. Int J Concr Struct Mater*   (2020) 14:14

Page 9 of 16

Figure 6i present that beam G09-GPC50 failed due to the crushing of concrete on the top surface under the load (compressive failure of the top concrete part). The beams in this particular type of failure recorded a large number of narrow cracks compared with the other failure mode conditions.

Figure 6l shows that beam G12-OPC35 failed due to the debonding of GFRP. This failure was due to the debonding of GFRP from the concrete at the bottom of the beam (cover part) and caused the propagation of horizontal cracks at the final stage of loading. This behaviour could be attributed to the localised failure of the GFRP bars at the cracks due to the sudden transfer of tensile forces from the fracturing concrete to the GFRP bars.

3.3 Load–Deflection Characteristics

Figure 7 shows the load–deflection curves at the midspan of the beam specimens. Generally, two important stages of behaviour were observed. The first stage was a linear branch with a steep slope, which is related to the un-cracked condition of the beam. This stage occurred when the cracking load was obtained, and a drop in the slope was observed due to the progressive cracking of the beam. The second stage was the settling of the cracking process, in which a nearly linear segment was observed until failure. A sudden drop in the load occurred in every

crack formation, which was more evident in load–deflection curves, especially for low reinforced beams. Even the number of cracks could be determined from the load–deflection curve instantly. In this work, all the beams were designed to fail in the flexure under the tensile mode, which was distinguished by the crack formation in the tensile stress zone. The FRP then ruptured under the compressive mode, which was characterised by the crushing of concrete.

3.3.1 Effect of Rebar Ratio

Figure 7 shows the load–deflection curves at the midspan of the beam specimens with the same concrete compressive strength and different rebar ratios. The rebar ratio affected the stiffness of the beam specimens, which appeared on their load–deflection behaviour. As expected, large deformations were obtained at low rebar ratios. By increasing ρ_f from $\rho_f < \rho_{fb}$ to $\rho_{fb} < \rho_f < 1.4\,\rho_{fb}$ and then to $\rho_f > 1.4\,\rho_{fb}$, the cracking load P_{cr} and ultimate load P_u increased compared with the beams with $\rho_f < \rho_{fb}$.

The cracking load increased by 9.3% and 172% and the ultimate load increased by 114.8% and 210.6% for beams with $f'_c = 20$ MPa and the GPC type, respectively (Fig. 7a). Also, the cracking load increased by 4.2% and 30.3% and the ultimate load increased by 146.6% and 248.3% for beams with $f'_c = 35$ MPa and the GPC type, respectively (Fig. 7b). Moreover, the cracking load increased by 13.7 and 23.5% and the ultimate load increased by 73.3% and 152.7% for beams with $f'_c = 50$ MPa and the GPC type, respectively (Fig. 7c). Furthermore, the cracking load increased by 29% and 34.8% and ultimate load increased by 146.8% and 302.9% for beams with $f'_c = 35$ MPa and the OPC type, respectively (Fig. 7d).

Regarding the increasing percentage in cracking and the ultimate load for both concrete types of beam specimens; GFRP-ROPC beams were more affected by the rebar ratio than GFRP-RGPC beams.

3.3.2 Effect of Concrete Compressive Strength

Figure 8 shows that the load–deflection curves at midspan of the tested beam specimens with the same cross-section, bar number, and concrete type would only vary in compressive strength. By increasing the concrete compressive strength, the deflection was decreased in the same corresponding load levels. The percentages of decrease varied, based on the rebar ratio. The ultimate load increased by 36.0% for beams with one bar (Fig. 8a), whereas the ultimate load increased by 2.1% and 8.0% for beams with two and three bars, respectively (Fig. 8b, c). Concrete compressive strength had a notable effect on the initial crack. Wherein the first cracking load increased with the compressive strength.
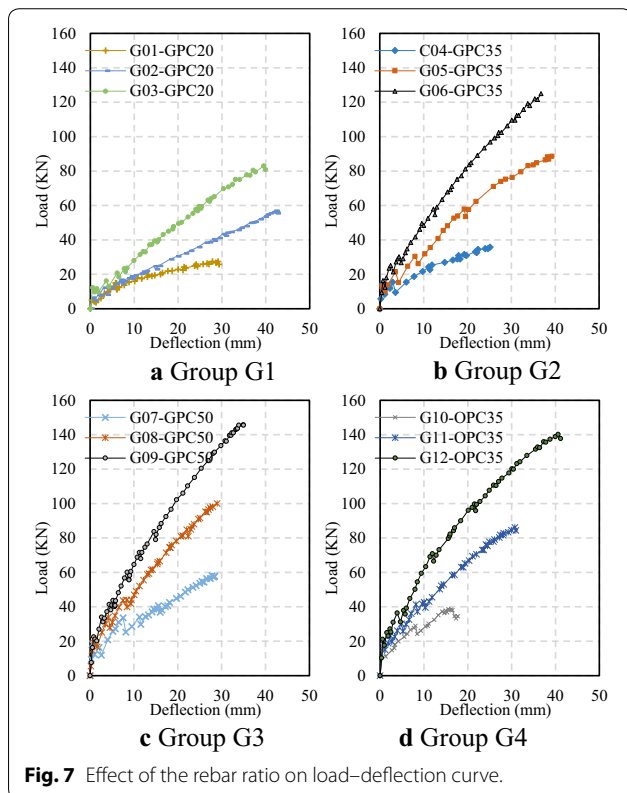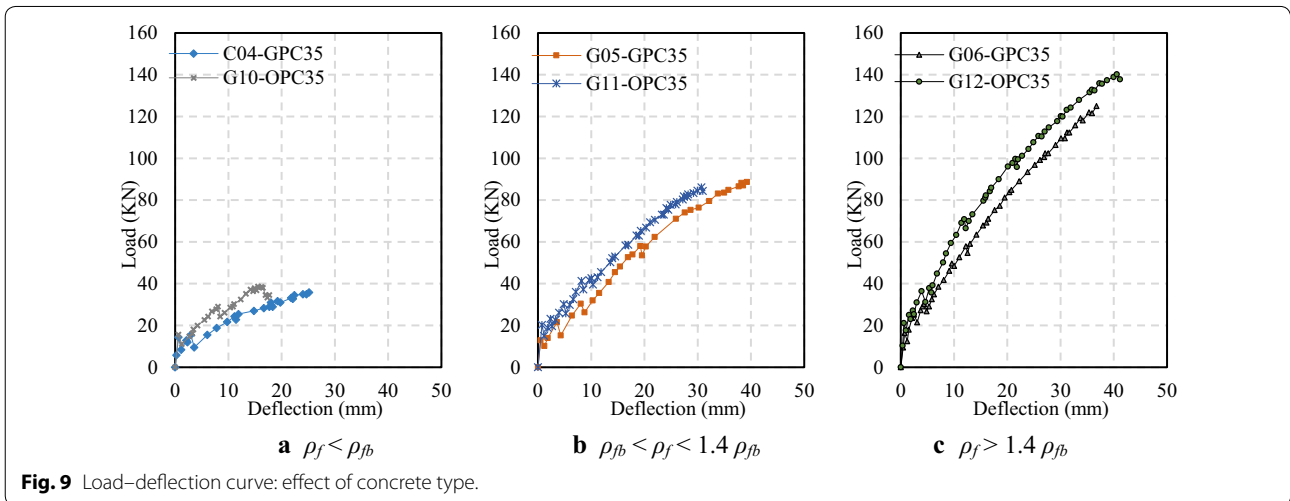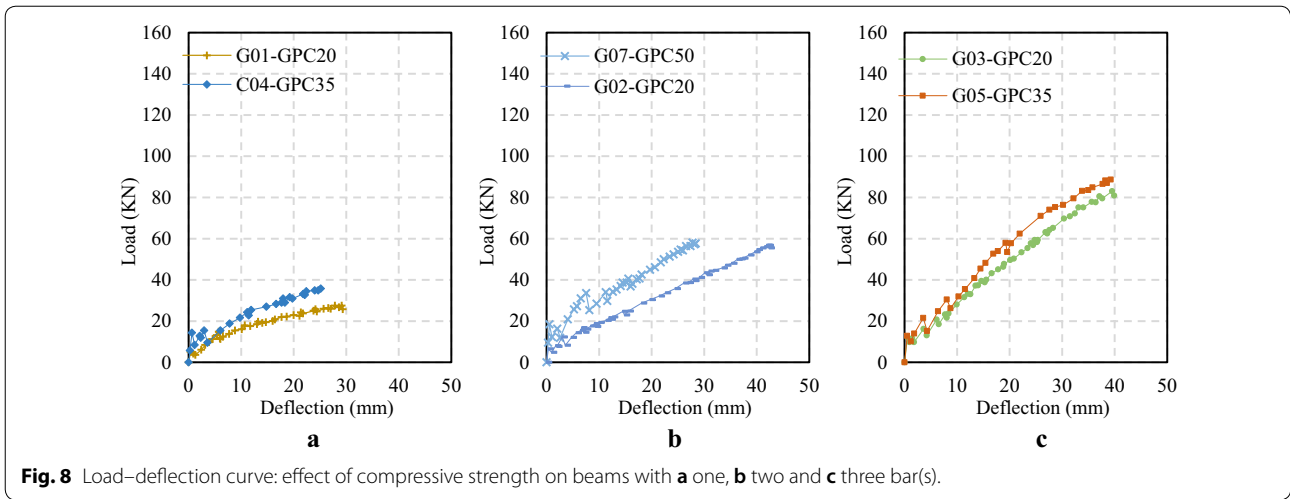

Fig. 7 Effect of the rebar ratio on load–deflection curve.

Ahmed *et al. Int J Concr Struct Mater*   (2020) 14:14

Page 10 of 16

Fig. 8 Load–deflection curve: effect of compressive strength on beams with **a** one, **b** two and **c** three bar(s).

Fig. 9 Load–deflection curve: effect of concrete type.

3.3.3 Effect of Concrete Type

Figure 9 shows the effect of concrete types (namely, GPC and OPC) for specimens with the same cross-section, compressive strength and rebar ratio. The recorded deflection of GPC was slightly higher than that of the same corresponding load levels. However, the ultimate load-carrying capacity of OPC was slightly higher (10.5%). Especially for beams with $\rho_f > 1.4\, \rho_{fb}$ than that of beams with $\rho_f < \rho_{fb}$ and $\rho_{fb} < \rho_f < 1.4\, \rho_{fb}$, wherein the load-carrying strength was approximately the same value at 4.4% with a 4.6% variance.

3.4 Crack Width, Number of Cracks, Concrete Strain and FRP Strain

Figure 10 shows the relation between crack width and the number of cracks, and Table 5 lists the number of cracks, crack width, concrete strain, and FRP strain. Higher crack width values were obtained for beams with low

Fig. 10 Relationship between the crack width and number of cracks.
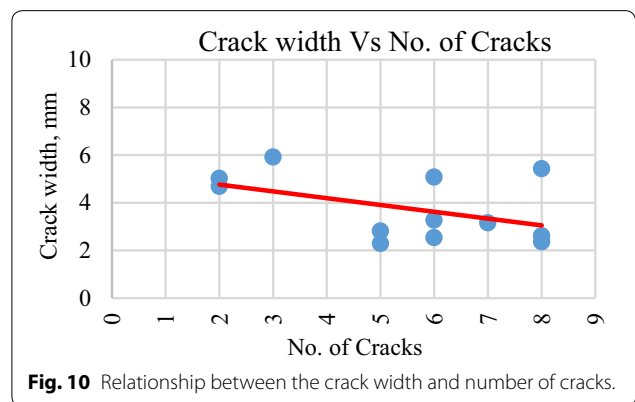
compressive strength, and GFRP-ROPC obtained higher crack width values than GFRP-RGPC beams. The relationship between the crack width and number of cracks

Ahmed *et al. Int J Concr Struct Mater* (2020) 14:14

Page 11 of 16

Table 5 Crack width, number of cracks, Concrete strain, and GFRP strain.

Beam ID	Crack width (mm)	Number of cracks	Concrete strain (Mm/Mm)	FRP strain (mm/mm)
G01-GPC20	5.92	3	0.0022	0.0247
G02-GPC20	5.43	8	0.0021	0.0241
G03-GPC20	5.08	6	0.0033	0.0253
G04-GPC35	5.02	2	0.0024	0.0250
G05-GPC35	3.27	6	0.0032	0.0242
G06-GPC35	3.16	7	0.0033	0.0222
G07-GPC50	2.81	5	0.0022	0.0247
G08-GPC50	2.54	6	0.0020	0.0186
G09-GPC50	2.61	8	0.0027	0.0166
G10-OPC35	4.69	2	0.0021	0.0261
G11-OPC35	2.29	5	0.0029	0.0257
G12-OPC35	2.36	8	0.0015	0.0200

indicated that beams with a large number of cracks obtained a low value of crack width. The number of cracks in the GFRP-RGPC and GFRP-ROPC beams was almost similar. Beams with a high rebar ratio obtained a large number of cracks and low values of crack width. As the ultimate loads reach the maximum limit for both GFRP-RGPC and GFRP-ROPC beams, the differences in max crack width were observed. The number of cracks in the GFRP-RGPC beams G04-GPC35, G05-GPC35 and G06-GPC35 were 2, 6 and 7 respectively which were the approximately same number of cracks that in the GFRP-ROPC beams G10-OPC35, G11-OPC35 and G12-OPC35 with the number of cracks 2, 5 and 8 respectively.

Indicating a good interaction between materials in one side and sufficient bond between GFRP bar and GPC on another side, the same as reported by (Maranan et al. 2014).

Figure 11 shows the Load–strain curves for different failure modes, wherein the first cracking and crack propagation could be visualised on the curves easily. For beam G07-GPC50, the strain in the GFRP bar nearly reached the ultimate strain whereas that in the GPC did not reach the ultimate strain, thereby indicating "tension failure of GFRP bars". For beam G08-GPC50, both strains were near the ultimate strain, thereby indicating "tension failure of GFRP bars followed by the compressive failure of the top concrete part". For beam G09-GPC50, the strain in the GPC nearly reached the ultimate strain, whereas that in the FRP bar did not, thereby indicating "compressive failure of the top concrete part". For beam G12-OPC35, neither strains reached the ultimate strain, thereby indicating failure by debonding of GFRP from the concrete at the bottom of the beam.

4 Theoretical Prediction

In this study, the theoretical flexural strength M_u of GFRP-RGPC and GFRP-ROPC beams were calculated, based on the equations provided by (ACI 440.1R-15 2015), (CSA S806–12 2012) and parabolic stress block method (Fig. 12). Then compared with the experimental flexural strength $M_{u, Exp}$.

4.1 Equations Provided by ACI 44.1R-15 and CSA S806-12

Based on (ACI 440.1R-15 2015), the flexural strength of a concrete beam reinforced with FRP bars can be calculated based on strain compatibility, internal force
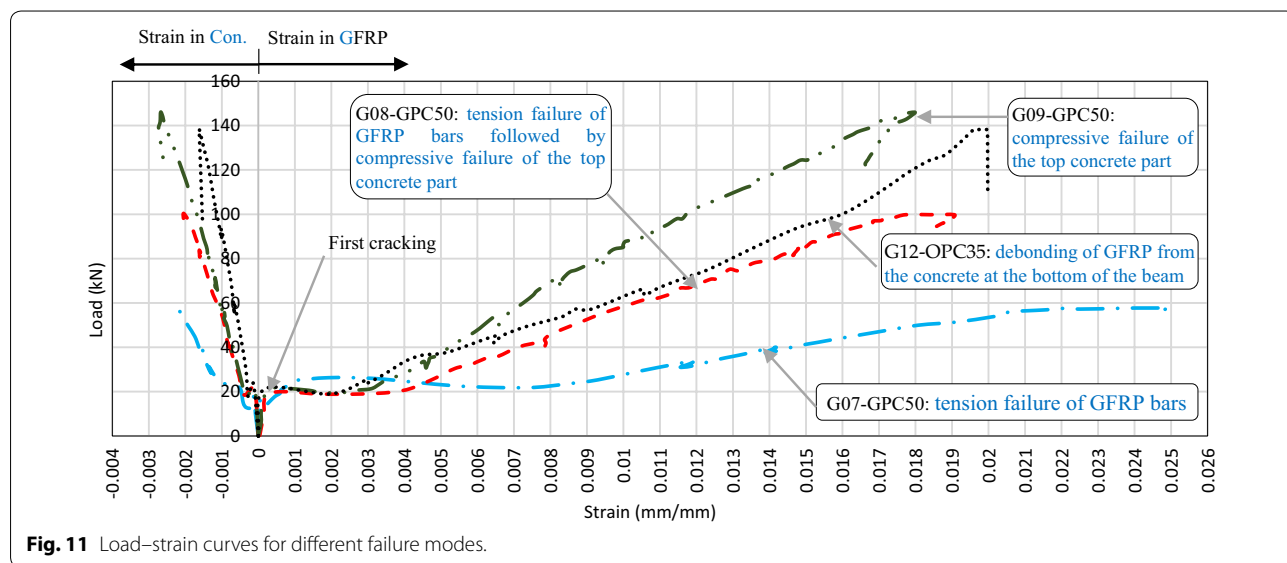

Fig. 11 Load–strain curves for different failure modes.

equilibrium, and control of the failure mode (tension failure of FRP bars or compressive failure of the top concrete part). The predicted failure modes can be determined by comparing the following; rebar ratio ρ_f (Eq. 1) to the balanced rebar ratio ρ_{fb} (Eq. 2), which indicates the rate of concrete crushing and FRP rupture. A_f is the area of the FRP bar, b is the width of the rectangular cross-section and d is the distance measured from the extreme compression fibre to the centroid of FRP bars. f'_c is the compressive strength of concrete, f_{fu} is the ultimate tensile stress of FRP bars, E_f is the elastic modulus of the FRP and ϵ_{cu} is the ultimate strain in concrete equal to 3%. Factor β_1 can be calculated from (Eq. 3).

Firstly, if $\rho_f > \rho_{fb}$, then the beam is considered over-reinforced, the controlling limit state is the compressive failure of the top concrete part. The flexural strength M_u can be calculated from (Eq. 4). f_f is the tensile stress of the FRP bars, which can be calculated from (Eq. 5).

Secondly, if $\rho_{fb} < \rho_f < 1.4\ \rho_{fb}$, then this particular condition is described by using a transition zone, wherein tension failure of FRP bars followed by the compressive failure of the top concrete part. Finally, if $\rho_f < \rho_{fb}$, then the beam is considered under-reinforced, wherein the controlling limit is the tension failure of FRP bars. M_u can be estimated using (Eqs. 6 and 7). c is the distance measured from the extreme compression fibre to the neutral axis.

Based on (CSA S806–12 2012), the FRP-reinforced concrete beams should be designed, such that the controlling limit state is the compressive failure of the top concrete part. ϵ_{cu} is equal to 3.5% and also depends on strain compatibility and internal force equilibrium. The balanced rebar ratio ρ_{fb} and factors $\alpha 1$ and $\beta 1$ can be calculated by using (Eqs. 8, 9 and 10), respectively. The flexural strength M_u, stress in the FRP bar f_f and the neutral axis c can be calculated by using (Eqs. 11, 12 and 13), respectively.

4.2 Parabolic stress block method

It is established the fact that the rising part of the stress–strain data for concrete material closely approximates a parabola (Jarquio 2004). Set of equations used for predicting the flexural strength ($M_{u,\ parabolic}$) of GFRP-RGPC and GFRP-ROPC beams based on the parabolic stress block, strain compatibility and internal force equilibrium. Figure 13 shows the basic parabola for ultimate strength analysis.

Figure 14a shows the balanced condition of compressive and tensile forces; the balanced rebar ratio ρ_{fb} can be found based on the (Eq. 14). c_b is the depth of the neutral axis when the maximum compressive strength achieved and can be calculated using the linear distribution of strains with respect to the neutral axis (Eq. 15). ϵ_{fu} is the ultimate strain of the GFRP bar.

Figure 14b shows the stress–strain distributions of the parabolic stress block method in a section at tension failure of GFRP bars. The criteria of this type of failure assume FRP ruptures before concrete crushing. Such a section is said to be under-reinforced. The strain in the FRP will be ϵ_{fu}, and the corresponding strain ϵ_c at the extreme compressive fibre will be less than the ultimate strain ϵ_{cu}. Strain at top ϵ_c, depth of the neutral axis c_t and compressive strength f_c corresponding to the top concrete strain ϵ_c can be calculated based on (Eqs. 16, 17, 18 and 19). The distance between the centroid of parabolic stress block and the neutral axis defined by x'. Which x' can be determined based on (Eq. 20). By taking the moment about the centroid of the compressive force, the proposed flexural strength $M_{u,\ Proposed}$ for tension failure of GFRP bars of GFRP-RGPC and GFRP-ROPC beams can be calculated based on the (Eq. 21).

Figure 14c shows the stress–strain distributions of the parabolic stress block method in a section at the compression failure of the top concrete part. The criteria of this type of failure assume that concrete is crushed before FRP rapture. The ratio of FRP in the compressive failure of the top concrete part is higher than the balanced ratio (over-reinforced). The same philosophy as the balanced case is used in the compressive failure of the top concrete part for calculating the FRP tensile stress f_f (Eq. 22). In which f_f is less than the ultimate strength f_{fu} and the distance from the extreme concrete fibre of maximum strain to the neutral axis at compression c_c (Eq. 23), respectively. By taking the moment about the centroid of the parabolic compressive force. The flexural strength $M_{u,\ Parabolic}$ for the compressive failure of the top concrete part of GFRP-RGPC and GFRP-ROPC beams can be determined based on (Eq. 24).

4.3 Comparison of Experimental Results with Theoretical Predictions

The predicted flexural strength was calculated on the basis of ($M_{u,\ ACI}$) of (ACI 440.1R-15 2015), ($M_{u,\ CSA}$) of (CSA S806–12 2012) and ($M_{u,\ parabolic}$) of the parabolic stress block method. Table 6 compares the experimental flexural strength (M_{u-Exp}) results. The prediction formulas provided by (ACI 440.1R-15 2015) and (CSA S806–12 2012) predicted the flexural strength of beams by 71.3% and 72.7% of the experimental results, respectively. While the parabolic stress block method predicted closely by 79.2% of the experimental results. (CSA S806–12 2012) Predicted high compressive strength values closely by 80.6% of the experimental results in comparison with (ACI 440.1R-15 2015) (75.6%), while the parabolic stress block method predicted closely by 87.3% of the experimental results, whereas the prediction values were significantly affected by the low rebar ratio, especially for
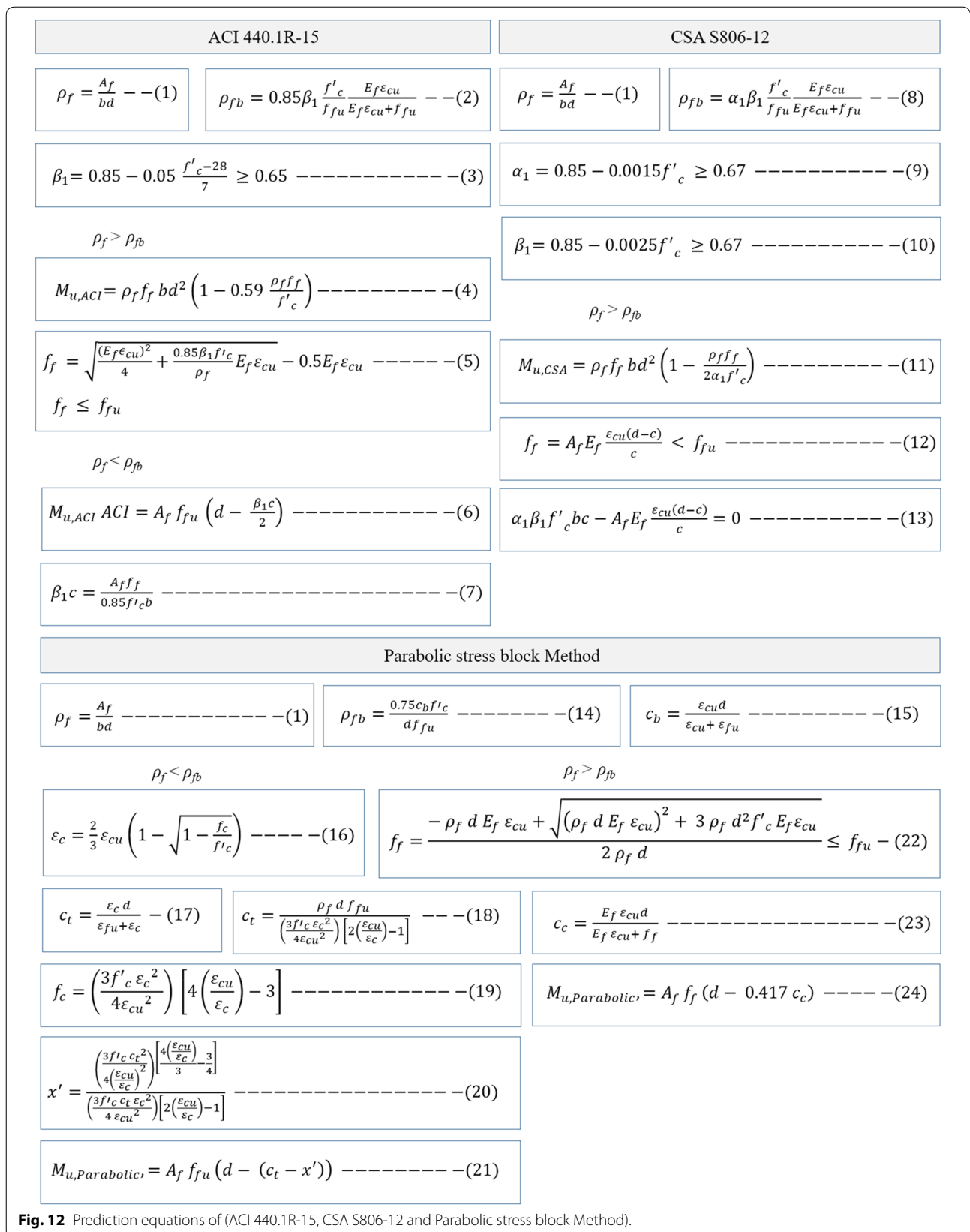
ACI 440.1R-15	CSA S806-12

$$\rho_f = \frac{A_f}{bd} \ ---(1)$$

$$\rho_{fb} = 0.85\beta_1 \frac{f'_c}{f_{fu}} \frac{E_f \varepsilon_{cu}}{E_f \varepsilon_{cu} + f_{fu}} \ ---(2)$$

$$\rho_f = \frac{A_f}{bd} \ ---(1)$$

$$\rho_{fb} = \alpha_1 \beta_1 \frac{f'_c}{f_{fu}} \frac{E_f \varepsilon_{cu}}{E_f \varepsilon_{cu} + f_{fu}} \ ---(8)$$

$$\beta_1 = 0.85 - 0.05 \frac{f'_c - 28}{7} \geq 0.65 \ ----------(3)$$

$$\alpha_1 = 0.85 - 0.0015 f'_c \geq 0.67 \ ----------(9)$$

$$\beta_1 = 0.85 - 0.0025 f'_c \geq 0.67 \ ----------(10)$$

$$\rho_f > \rho_{fb}$$

$$M_{u,ACI} = \rho_f f_f bd^2 \left(1 - 0.59 \frac{\rho_f f_f}{f'_c}\right) ----------(4)$$

$$\rho_f > \rho_{fb}$$

$$M_{u,CSA} = \rho_f f_f bd^2 \left(1 - \frac{\rho_f f_f}{2\alpha_1 f'_c}\right) ----------(11)$$

$$f_f = \sqrt{\frac{(E_f \varepsilon_{cu})^2}{4} + \frac{0.85\beta_1 f'_c}{\rho_f} E_f \varepsilon_{cu}} - 0.5 E_f \varepsilon_{cu} \ ------(5)$$

$$f_f \leq f_{fu}$$

$$f_f = A_f E_f \frac{\varepsilon_{cu}(d-c)}{c} < f_{fu} \ -------------(12)$$

$$\rho_f < \rho_{fb}$$

$$M_{u,ACI} \ ACI = A_f f_{fu} \left(d - \frac{\beta_1 c}{2}\right) -----------(6)$$

$$\alpha_1 \beta_1 f'_c bc - A_f E_f \frac{\varepsilon_{cu}(d-c)}{c} = 0 \ -----------(13)$$

$$\beta_1 c = \frac{A_f f_f}{0.85 f'_c b} \ ----------------(7)$$

Parabolic stress block Method

$$\rho_f = \frac{A_f}{bd} \ ---------------(1)$$

$$\rho_{fb} = \frac{0.75 c_b f'_c}{d f_{fu}} \ --------(14)$$

$$c_b = \frac{\varepsilon_{cu} d}{\varepsilon_{cu} + \varepsilon_{fu}} \ ----------(15)$$

$$\rho_f < \rho_{fb}$$

$$\varepsilon_c = \frac{2}{3} \varepsilon_{cu} \left(1 - \sqrt{1 - \frac{f_c}{f'_c}}\right) -----(16)$$

$$\rho_f > \rho_{fb}$$

$$f_f = \frac{-\rho_f d E_f \varepsilon_{cu} + \sqrt{\left(\rho_f d E_f \varepsilon_{cu}\right)^2 + 3 \rho_f d^2 f'_c E_f \varepsilon_{cu}}}{2 \rho_f d} \leq f_{fu} - (22)$$

$$c_t = \frac{\varepsilon_c d}{\varepsilon_{fu} + \varepsilon_c} - (17)$$

$$c_t = \frac{\rho_f d f_{fu}}{\left(\frac{3 f'_c \varepsilon_c^2}{4 \varepsilon_{cu}^2}\right) \left[2\left(\frac{\varepsilon_{cu}}{\varepsilon_c}\right) - 1\right]} \ ---(18)$$

$$c_c = \frac{E_f \varepsilon_{cu} d}{E_f \varepsilon_{cu} + f_f} \ ------------------(23)$$

$$f_c = \left(\frac{3 f'_c \varepsilon_c^2}{4 \varepsilon_{cu}^2}\right) \left[4\left(\frac{\varepsilon_{cu}}{\varepsilon_c}\right) - 3\right] -------------(19)$$

$$M_{u,Parabolic,} = A_f f_f (d - 0.417 c_c) -----(24)$$

$$x' = \frac{\left(\frac{3 f'_c c_t^2}{4\left(\frac{\varepsilon_{cu}}{\varepsilon_c}\right)^2}\right) \left[\frac{4\left(\frac{\varepsilon_{cu}}{\varepsilon_c}\right)}{3} - \frac{3}{4}\right]}{\left(\frac{3 f'_c c_t \varepsilon_c^2}{4 \varepsilon_{cu}^2}\right) \left[2\left(\frac{\varepsilon_{cu}}{\varepsilon_c}\right) - 1\right]} \ ------------------(20)$$

$$M_{u,Parabolic,} = A_f f_{fu} \left(d - (c_t - x')\right) --------(21)$$

Fig. 12 Prediction equations of (ACI 440.1R-15, CSA S806-12 and Parabolic stress block Method).
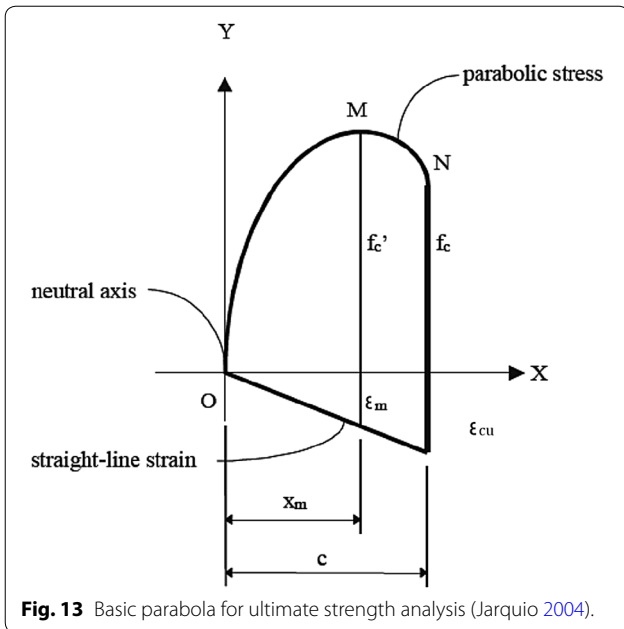
Fig. 13 Basic parabola for ultimate strength analysis (Jarquio 2004).

$\rho_f < \rho_{fb}$. Beams C01-GPC20, C04-GPC35, C07-GPC50 and C10-OPC35 did not satisfy the limit state condition (concrete crushing) provided by (CSA S806–12 2012).
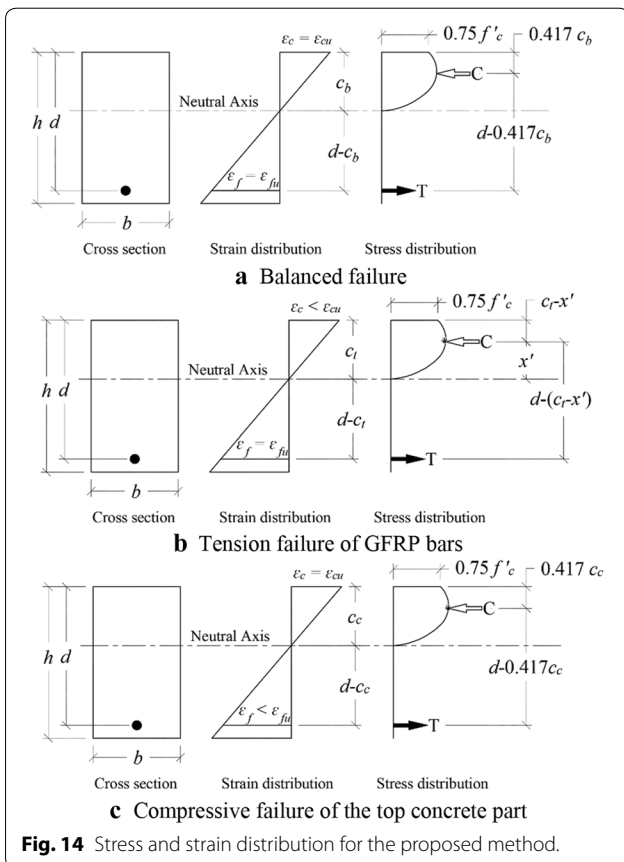

Fig. 14 Stress and strain distribution for the proposed method.

Figure 15 shows a graphical comparison of the flexural capacities provided by (ACI 440.1R-15 2015), (CSA S806–12 2012), the parabolic stress block method and the experimental results.

5 Conclusions

The flexural strength and behaviour of GFRP-RGPC and GFRP-ROPC beams were investigated by using a four-point bending test. Based on the experimental outcomes, the following conclusions can be drawn.

1. Four different types of failure were observed. Tension failure of GFRP bars for beams reinforced with $\rho_f < \rho_{fb}$, tension failure of GFRP bars followed by a compressive failure of the top concrete part, compressive failure of the top concrete part for beams reinforced with $\rho_f > \rho_{fb}$ and debonding of GFRP from the concrete at the bottom of the beam.
2. The rebar ratio affected the stiffness of the beam specimens. Consequently, the beams with low rebar ratio recorded significant deformation and the ultimate load enhancement (73.3%–302.9%) was recorded with increasing rebar ratio with respect to their load–deflection behaviour. GFRP-ROPC beams were more affected by increasing the rebar ratio than GFRP-RGPC beams.
3. The compressive strength had a significant effect on the initial crack. The initial cracking load increased with the compressive strength (4.2%–172%). Beams with lower concrete compressive strength had more deflections, in comparison with higher compressive strength beams. When new cracks appeared, a sudden reduction of the load was observed for the beams with high compressive strength.
4. The GFRP-RGPC beams had more deflection than GFRP-ROPC beams at the same corresponding load level. The ultimate load-carrying capacity of GFRP-ROPC beams was slightly higher (10.5%). Especially for beams with $\rho_f > 1.4\,\rho_{fb}$; however, for beams with $\rho_f < \rho_{fb}$ and $\rho_{fb} < \rho_f < 1.4\,\rho_{fb}$, the load-carrying capacity was approximately the same value at 4.4% with a 4.6% variance.
5. The crack width recorded high values for beams with low compressive strength, and the beams with a large number of cracks recorded a low value of crack width.
6. The number of cracks in the GFRP-RGPC beams was nearly the same as in the GFRP-ROPC beams. The beams with higher rebar ratios obtained a larger number of cracks and lower crack width values. Thus, the GFRP-RGPC beams obtained a higher value of crack width compared with GFRP-ROPC beams.

Table 6 Comparison of theoretical prediction and experimental results.

Group	Beam ID	Flexural capacity				Comparisons %					
		$M_{u\text{-}Exp}$ (kN m)	$M_{u,ACI}$ (kN m)	$M_{u,CSA}$ (kN m)	$M_{u,Parabolic}$ (kN m)	$M_{u,ACI}/M_{u\text{-}Exp}$		$M_{u,CSA}/M_{u\text{-}Exp}$		$M_{u,Parabolic}/M_{u\text{-}Exp}$	
G1	G01-GPC20	10.52	9.48	N/C	9.42	90.1	74.5	N/C	70.1	89.5	81.6
	G02-GPC20	22.6	16.49	17.36	18.52	73.0		76.8		81.9	
	G03-GPC20	32.68	19.78	20.75	24.03	60.5		63.5		73.5	
G2	G04-GPC35	14.32	9.58	N/C	9.41	66.9	66.0	N/C	70.7	65.7	73.8
	G05-GPC35	35.32	25.22	27.26	27.78	71.4		77.2		78.7	
	G06-GPC35	49.88	29.77	32.01	38.57	59.7		64.2		77.3	
G3	G07-GPC50	23.08	19.05	N/C	18.82	82.5	75.6	N/C	80.6	81.5	87.3
	G08-GPC50	40	32.41	36.23	37.04	81.0		90.6		92.6	
	G09-GPC50	58.32	36.97	41.14	51.31	63.4		70.5		88.0	
G4	G10-OPC35	13.68	9.58	N/C	9.41	70.0	69.1	N/C	69.4	68.8	74.3
	G11-OPC35	33.76	26.92	27.26	28.45	79.7		80.7		84.3	
	G12-OPC35	55.12	31.72	32.01	38.57	57.5		58.1		70.0	
					Average	71.3		72.7		79.2	

N/C not-calculated because (CSA S806–12 2012) considers (concrete crushing) as the only controlling limit state.

Fig. 15 Graphical comparison of predicted and experimental flexural strength of beams.
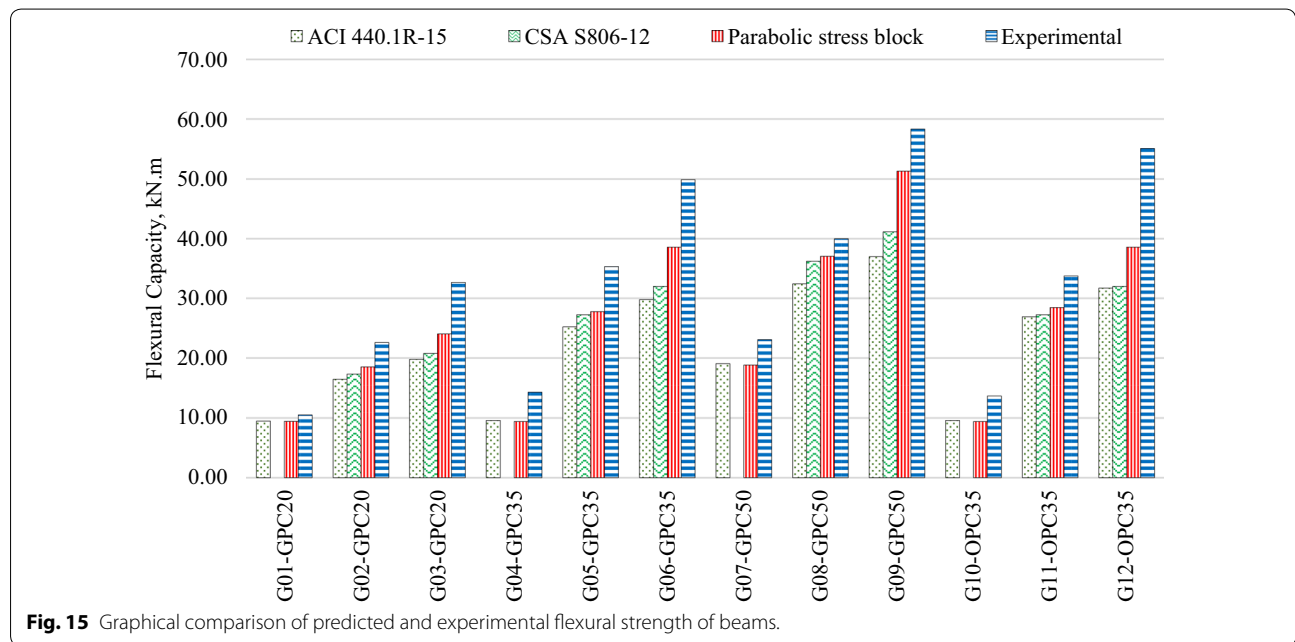
7. The prediction equations provided by (ACI 440.1R-15 2015) and (CSA S806–12 2012) predicted the flexural strength of the beams by 71.3% and 72.7% of the experimental results, respectively. The parabolic stress block method predicted closely by 79.2% of the experimental results.

Abbreviations
OPC: ordinary Portland concrete; GPC: geopolymer concrete; FRP: fibre-reinforced polymer; GFRP: glass fibre-reinforced polymer; SROPC: steel-reinforced ordinary portland concrete; SRGPC: steel-reinforced geopolymer concrete; GFRP-RGPC: glass fibre-reinforced polymer-reinforced geopolymer concrete; GFRP-ROPC: glass fibre-reinforced polymer-reinforced ordinary portland concrete.

Ahmed *et al. Int J Concr Struct Mater* (2020) 14:14

Page 16 of 16

References
Abraham, R., Raj, S., & Abraham, V. (2013). Strength and behaviour of geopolymer concrete beams. *International Journal of Innovative Research in Science, Engineering and Technology, 2*(1), 159–166.

ACI 440.1R-15. (2015). *Guide for the design and construction of Concrete Reinforced with Fiber Reinforced Polymers (FRP) bars, ACI Committee 440.* Farmington Hills, MI, USA: American Concrete Institute.

Ascione, L., Mancusi, G., & Spadea, S. (2010). Flexural behaviour of concrete beams reinforced with GFRP bars. *Strain, 46*(5), 460–469. https://doi.org/10.1111/j.1475-1305.2009.00662.x.

ASTM C 39/C 39M. (1999). *Standard test method for compressive strength of cylindrical concrete specimens.* West Conshohocken, PA, USA: ASTM International.

ASTM C 469/C 469M. (2014). *Standard test method for static modulus of elasticity and Poisson's Ratio of Concrete in compression.* West Conshohocken, PA, USA: ASTM International.

ASTM C 496/C 496m. (2004). *Standard Test method for splitting tensile strength of cylindrical concrete specimens.* West Conshohocken, PA, USA: ASTM International.

ASTM C 78/C 78M. (2013). *Standard test method for flexural strength of concrete (using simple beam with third-point loading).* West Conshohocken, PA, USA: ASTM International.

CSA S806-12. (2012). *Design and construction of Building structures with Fiber-Reinforced Polymers, Canadian Standard Association (CSA).* Canada: Ontario.

Davidovits, J. (1988). Geopolymer chemistry and properties. In *Proceedings of the 1st international conference on geopolymer '88* (Vol. 1, pp. 25–48). Compiegne, 1–3 June 1988.

Davidovits, J. (1994). Geopolymers: man-made rock geosynthesis and the resulting development of very early high strength cement. *Journal of Materials education, 16,* 91–139.

Duxson, P., Provis, J. L., Lukey, G. C., & Van Deventer, J. S. J. (2007). The role of inorganic polymer technology in the development of 'green concrete'. *Cement and Concrete Research, 37*(12), 1590–1597. https://doi.org/10.1016/j.cemconres.2007.08.018.

Fico, R. (2007) Limit States Design of Concrete Structures Reinforced with FRP Bars.), vol. PhD Thesis, University of Naples Federico II, Naples, Italy.

Hardjito, D. & Rangan, B. V. (2005) *Development and Properties of Low-Calcium Fly Ash-based Geopolymer Concrete. Faculty of Engineering Curtin University of Technology Perth, Australia.* Report GC1, pp. 1–94. http://hdl.handle.net/20.500.11937/5594.

Hardjito, D. & Wallah, S. E. (2005) Introducing Fly Ash-based Geopolymer Concrete Manufacture and Engineering Properties In *Proceedings of 30th Conference on Our World in Concrete & Structures: 23-24, Singapore.*

Hutagi, A. & Khadiranaikar, R. (2016) Flexural behavior of reinforced geopolymer concrete beams In *Proceedings of 2016 International Conference on Electrical, Electronics, and Optimization Techniques (ICEEOT).* IEEE, pp. 3463–3467.

Jarquio, R. V. (2004). *Analytical Method in Reinforced Concrete.* Boca Raton: Universal Publishers.

Kar, A., Ray, I., Halabe, U. B., Unnikrishnan, A., & Dawson-Andoh, B. (2014). Characterizations and quantitative estimation of alkali-activated binder paste from microstructures. *International Journal of Concrete Structures Materials, 8*(3), 213–228.

Khale, D., & Chaudhary, R. (2007). Mechanism of geopolymerization and factors influencing its development: a review. *Journal of Materials Science, 42*(3), 729–746. https://doi.org/10.1007/s10853-006-0401-4.

Kotwal, A. R., Kim, Y. J., Hu, J., & Sriraman, V. (2015). Characterization and early age physical properties of ambient cured geopolymer mortar based on class C fly ash. *International Journal of Concrete Structures and Materials, 9*(1), 35–43.

Kumar, B. S. C. & Ramesh, K. (2017) Flexural Behavior of Reinforced Geopolymer Concrete Beams with GGBS and Metakaolin. *Global Journal of Engineering Science and Researches* **4**.

Kumaravel, S. & Thirugnanasambandam, S. (2013) Flexural behaviour of reinforced low calcium fly ash based geopolymer concrete beam. *Global Journal of Research In Engineering.*

Lee, W. K. W., & Van Deventer, J. S. J. (2002). Structural reorganisation of class F fly ash in alkaline silicate solutions. *Colloids and Surfaces A: Physicochemical and Engineering Aspects, 211*(1), 49–66. https://doi.org/10.1016/S0927-7757(02)00237-6.

Lloyd, N. A. & Rangan, B. V. (2010) Geopolymer concrete: a review of development and opportunities. In *the Proceedings of 35th conference on our world in concrete and structures, Singapore Concrete Institute, Singapore.*), pp. 25-27.

Luhar, S., Chaudhary, S., & Luhar, I. (2019). Development of rubberized geopolymer concrete: Strength and durability studies. *Construction and Building Materials, 204,* 740–753. https://doi.org/10.1016/j.conbuildmat.2019.01.185.

Madhava, T. V., Manjunath, G., & Venugopal, K. (2013). Phenomenological Model to Re-proportion the Ambient Cured Geopolymer Compressed Blocks. *International Journal of Concrete Structures Materials, 7*(3), 193–202.

Madheswaran, C. K., Ambily, P. S., Rajamane, N. P., & Arun, G. (2014). Studies on flexural behaviour of reinforced geopolymer concrete beams with lightweight aggregates. *International Journal of Civil and Structural Engineering, 4*(3), 295. https://doi.org/10.6088/ijcser.201304010029.

Maranan, G., Manalo, A., Benmokrane, B., Karunasena, W. & Mendis, P. J. a. S. J. (2017) Shear Behavior of Geopolymer Concrete Beams Reinforced with Glass Fiber-Reinforced Polymer Bars **114(2)**.

Maranan, G. B., Manalo, A. C., Benmokrane, B., Karunasena, W., & Mendis, P. (2015). Evaluation of the flexural strength and serviceability of geopolymer concrete beams reinforced with glass-fibre-reinforced polymer (GFRP) bars. *Engineering Structures, 101,* 529–541. https://doi.org/10.1016/j.engstruct.2015.08.003.

Maranan, G., Manalo, A., Karunasena, K., & Benmokrane, B. (2014). Bond stress-slip behavior: case of GFRP bars in geopolymer concrete. *Journal of Materials in Civil Engineering, 27*(1), 04014116. https://doi.org/10.1061/(ASCE)MT.1943-5533.0001046.

Mccaffrey, R. (2002) Climate change and the cement industry. *Global cement and lime magazine (Environmental special issue):*15–19.

Mehta, P. K. (2001). Reducing the environmental impact of concrete. *Concrete International, 23*(10), 61–66.

Thangamanibindhu, M. K., & Murthy, D. S. R. (2015). Flexural Behavior of Reinforced Geopolymer Concrete Beams partially replaced with Recycled Coarse Aggregates. *International Journal of Civil Engineering and Technology (IJCIET), 6*(7), 13–23.

Theriault, M., & Benmokrane, B. (1998). Effects of FRP reinforcement ratio and concrete strength on flexural behavior of concrete beams. *Journal of composites for construction, 2*(1), 7–16.

Wu, W. P. (1990) Thermomechanical Properties of Fiber Reinforced Plastic (FRP) Bars.) PhD Thesis, West Virginia University, Morgantown, West Virginia, USA.

Xu, H., & Van Deventer, J. S. J. (2002). Geopolymerisation of multiple minerals. *Minerals Engineering, 15*(12), 1131–1139. https://doi.org/10.1016/S0892-6875(02)00255-8.

Publisher's Note
Springer Nature remains neutral with regard to jurisdictional claims in published maps and institutional affiliations.